Preparation of Ultra-Thin PAN-Based Activated Carbon Fibers with Physical Activation

Yen-Ju Su, Tes-Hao Ko, Jui-Hsiang Lin

Department of Material Science and Engineering, Feng Chia University, Taichung 40724, Taiwan

Received 27 September 2007; accepted 10 January 2008
DOI 10.1002/app.27982
Published online 6 March 2008 in Wiley InterScience (www.interscience.wiley.com).

ABSTRACT: This study elucidates the stabilization and activation in forming activated carbon fibers (ACFs) from ultra-thin polyacrylonitrile (PAN) fibers. The effect of stabilization time on the properties and structure of resultant stabilized fibers was investigated by thermal analysis, X-ray diffraction (XRD), elemental analysis, and scanning electron microscopy (SEM). Stabilization was optimized by the pyrolysis of ultra-thin PAN fibers in air atmosphere at 280°C for 15 min, and subsequent activation in steam at 1000°C for 0.75 to 15 min. Resultant ACFs were characterized by N_2 adsorption at 77 K to evaluate pore parameters, XRD to evaluate structure parameters, and field emission scanning electron microscopy (FESEM) to elucidate surface morphology. The produced ACFs had surface areas of 668–1408 m^2/g and a micropore volume to total pore volume ratio from 78 to 88%. Experimental results demonstrate the surface area and micropore volume of 1408 m^2/g and 0.687 cm^3/g, respectively, following activation at 1000°C for 10 min. J Appl Polym Sci 108: 3610–3617, 2008

Key words: stabilization; fibers; pyrolysis; surface; polyacrylontrile

INTRODUCTION

Porous carbon materials have been increasingly studied in recent years. Forms of porous materials include conventional activated carbon bulk,[1] activated carbon fibers (ACFs),[2] and fine carbon particles.[3] The development of novel adsorbents with fibrous morphologies, such as ACFs has attracted increasing interest. ACFs have excellent adsorption properties and therefore have a very important role in numerous areas of modern science and technology. ACFs have various advantages over traditional granular activated carbons; they include a small diameter (minimizing diffusion limitation and allowing rapid adsorption or desorption), a narrower pore size distribution, and better adsorption capacity at low adsorbate concentration than conventionally activated granular carbons.

ACFs have been extensively applied in fields such as water treatment,[4] removal of SO_x, NO_x,[5] and toxic gases.[6] Recently, the use of ACFs in new areas such as methane storage and polarizable electrode[7] has attracted considerable interest. However, one shortcoming must be overcome before ACFs can be employed in various fields, i.e., its high production cost. ACF is generated via a series of processes, including stabilization, carbonization, and activation. The selection of raw material is essential in generating high-quality ACFs. Polyacrylonitrile (PAN),[8] coal and petroleum-based pitches,[9] cellulose,[10] and phenolic resin[11] have been used as raw precursor fiber materials from various candidates. ACFs are characterized by large internal surface areas and high degrees of porosity. Porosity develops during activation, because of partial gasification in steam and/or carbon dioxide, and is governed by numerous factors, including degree of activation and the conditions of carbonization.[12] While the porous structure of resulting ACFs depends mainly on the activation agents and activation condition, the nature of the raw material significantly influences the properties of product. ACF is a carbonaceous adsorbent that has slit-shaped micropores, which is the source of their high adsorption capacity which makes them effective adsorbents, catalysts, and catalyst supports. Such traits are associated with their porosity and surface structural characteristics. PAN-based ACFs contain nitrogen, which is responsible for adsorbent and catalytic functions.[13]

In this investigation, pyrolysis with air and physical activation with steam were performed, using ultra-thin PAN fibers as the starting material. Such ACFs prepared by varying the activation time were investigated by X-ray diffractometer (XRD), FESEM, and nitrogen adsorption testing. These analytic approaches are expected to help us understand the relationship between the microstructure and the properties of ultra-thin PAN-based ACFs that were prepared under various activation conditions.

Correspondence to: Y.-J. Su (keigosuru@yahoo.com.tw).
Contract grant sponsor: Biomedical and Technical Fibers Department of Industrial Technology Research Institute.

Journal of Applied Polymer Science, Vol. 108, 3610–3617 (2008)

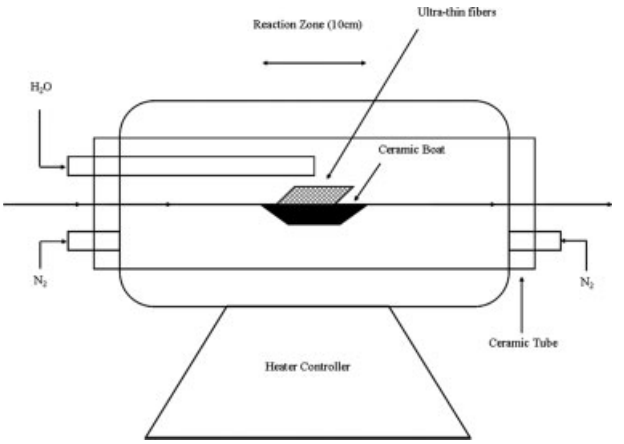

Figure 1 Schematic drawing showing process of ACFs from oxidized fibers.

EXPERIMENTAL

Sample preparation

Ultra-thin PAN fibers with mean diameters of ~ 4.75 μm, supplied by the Industrial Technology Research Institute, were polymerized from acrylonitrile (~ 85%) and vinyl acetate (~ 10%) monomers and used as precursors to yield ACFs. Stabilization was attained at a constant zone furnace temperature (280°C) for 15, 30, and 60 min in air atmosphere at a heating rate of 2°C/min. Stabilized fibers were activated by passing them through a ceramic reaction tube (Fig. 1). Based on the preliminary experiment and the research of Ko et al.,[14] the activation was carried out by heating the stabilized fibers in H_2O at 1000°C between 0.75 and 15 min.

Nitrogen adsorption measurements

A Micromeritics ASAP 2020 surface area and porosimetry apparatus (Micrometics, Norcross, GA) was used to make volumetric measurements to plot the nitrogen adsorption isotherms at 77 K at relative pressure from 10^{-6} to 1. Highly pure (99.999%) nitrogen was used; before measurement, all the samples were degassed at 300°C for 6 h. Nitrogen adsorption experiments were performed in static mode using a mass flow controller that was programmed to supply nitrogen at a fixed rate to a sample container. Following equilibration, the pressure was recorded and the process continued at higher pressures up to the saturation pressure. The difference between the preceding and the following equilibrated pressure, along with the dose volume, was used to calculate the amount of nitrogen adsorbed by a sample. The Brunauer-Emmett-Teller (BET) procedure[15] was utilized to specify the surface area, and the *t*-plot method[16] yielded the microporous volume and the mesoporous surface.

Sample characterization

The morphology of PAN and oxidized fibers was observed under a HITACHI S3000 scanning electron microscope (SEM). Fibers initially underwent carbon coating, and then were imaged and photographed under a SEM at potentials of 10–15 kV. The ACF morphology was observed under a HITACHI S-4800 field emission scanning electron microscope (FESEM). An SDT 2960 thermal analyzer with simultaneous DSC-TGA was utilized to investigate the reaction of the PAN precursor. The mass of the sample was 3 mg, and the sample was heated at 10°C /min to 500°C in an atmosphere of air. A Rigaku X-ray diffractometer, providing Ni-filtered Cu Kα radiation, was used to measure the crystalline-related properties of the samples. The step-scan method was utilized to determine the *d* spacing and the stacking size (*Lc*, stacking height of layer planes) of ACFs and the aromatization index (AI) of stabilized fibers. The Scherrer equation determines the stacking size from width of (002) reflection *B*, which increases as the stacking size declines as follows:

$$Lc = \frac{k\lambda}{B\cos\theta},$$

where $\lambda = 0.154$ nm, k is an apparatus constant (=1.0), and B is the half width of (002) broadened reflection. An AccuPyc 1330 Pynometer was used to analyze the density of all samples, and the ideal gas law was applied to determine the sample volume, given known volumes of the sample chamber and the gas reservoir and a change in pressure. The sample volume is translated into an absolute density (weight known), and a Perkin–Elmer 240CEA was used for elemental analysis. All the stabilized and activated samples were analyzed to identify carbon, hydrogen, and nitrogen, while the oxygen content was determined by the difference.

RESULTS AND DISCUSSION

Properties of stabilized fibers

The degradation of PAN during stabilization is always linked with large exotherms. Fitzer and Müller[17] made differential thermal analysis measurements to investigate the cyclization and stabilization kinetics of PAN that was heat-treated in air and nitrogen, and cyclization was identified as a first-order reaction. Polymerization is caused by the stabilization of a PAN fiber in an inert or an oxidizing atmosphere and yields a thermally stable cyclized structure that is known as a ladder polymer. Figure 2 presents the results of differential scanning calorimetry (DSC) of PAN precursor fibers. An exothermic reaction begins at ~ 150°C. This reaction proceeds

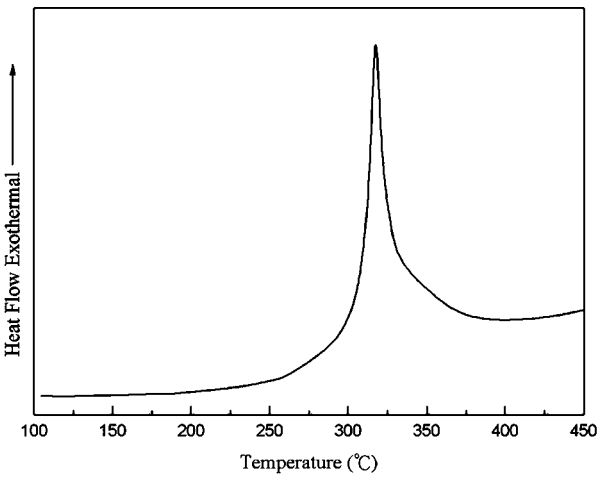

Figure 2 DSC curve of ultra-thin PAN fibers (heating rate: 10°C/min, in air).

slowly as the temperature rises to 250°C, and then rapidly to 318°C (which is the fusion temperature associated with the formation of ladder polymer). Based on DSC, the stabilization temperature was set to 280°C. If when the oven temperature was set to below 180°C, the fibers were not sufficiently thermally stabilized to the central part of the fiber. Moreover, the temperature could not be set above the fusing temperature of the precursor; high-temperature stabilization causes the over-absorption of oxygen. These reactions worsened the mechanical properties and the defects in microstructure.

Figure 3 depicts the morphology of PAN fibers and the distribution of ultra-thin PAN diameters (4.4–5.0 μm, average 4.75 μm). Before stabilization, smooth surfaces are found on the PAN fiber surfaces and then turn to rough surface with holding time during stabilization. Because of the degradation of

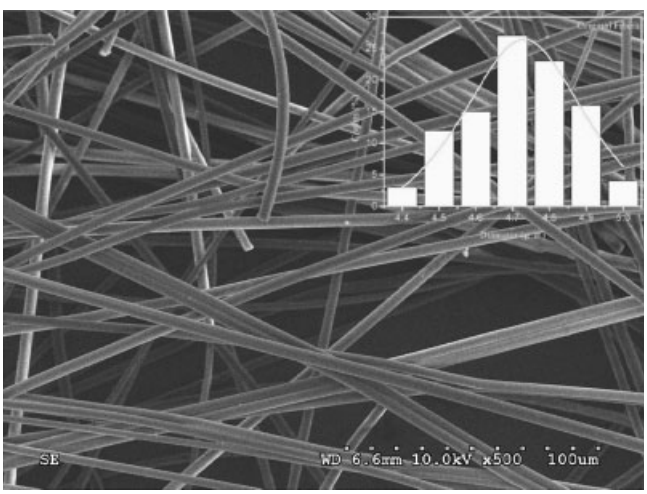

Figure 3 SEM image of ultra-thin PAN fibers.

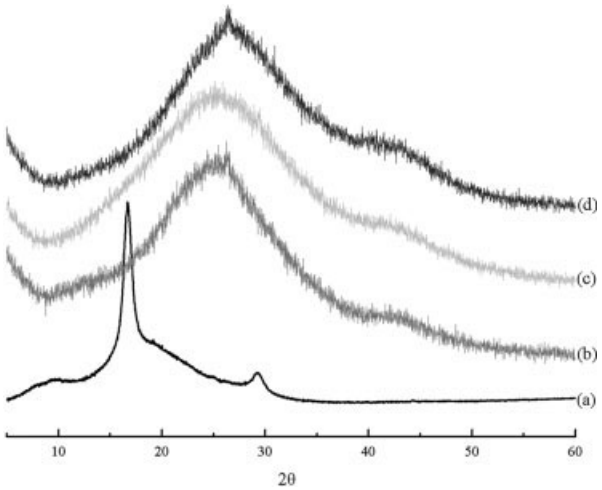

Figure 4 Wide-angle diffraction patterns for ultra-thin PAN fibers: (a) original, (b) stabilized at 15 min, (c) stabilized at 30 min, and (d) stabilized at 60 min.

PAN fibers during stabilization, it is always associated with a large exotherm (Fig. 2). Therefore, the pyrolysis processes will promote cyclization, shrinkage, and lead to formation of roughness surface. Some connection exists between the optimal time of stabilization and the fiber diameter. Thermal analysis yielded results from a stabilization time of 15–60 min at 280°C.

XRD studies of PAN fibers yielded two diffraction peaks at Bragg angles of $2\theta = 17^\circ$ and 29°, as presented in Figure 4. When the treatment temperature exceeded 180°C, the X-ray intensity at $2\theta = 17^\circ$ declined slowly, and a new peak appeared at $2\theta = 25^\circ$, corresponding to a sheet-like structure ladder polymer. Uchida et al.[18] attributed the new reflection to the structure of an aromatized ladder polymer and introduced the ''aromatization index,'' as follows:

$$\mathrm{AI}\ (\%) = \frac{I_a}{I_a + I_p}$$

where I_a is the diffraction intensity associated with the aromatic structure (ladder polymer) at around $2\theta = 25^\circ$ and I_p is the diffraction from the PAN crystal at around $2\theta = 17^\circ$. The AI value increases with temperature or heat-treatment time during stabilization.[14,18] Ko et al.[14] modified the testing method and recommended that the AI value can be used to check the stabilization process and estimate amount of the ladder polymer. When the PAN fiber is heated above 180°C in the presence of oxygen, C≡N bonds are converted into C=N bonds as the ladder polymer is formed. The percentage conversion of C≡N to C=N groups depends on the extent of stabilization.

TABLE I
Properties of PAN and Stabilized Fibers

Stabilization time (min)	Density (g/cm^3)	AI (%)	Carbon content (%)	Oxygen content (%)	Average diameter (μm)
0[a]	1.173	–	42.1	10.6	4.75
15	1.343	58.68	65.7	10.8	4.47
30	1.427	61.89	63.4	13.2	4.25
60	1.462	63.52	60.1	15.2	4.11

[a] Properties of fibers obtained from starting materials (ultra-thin PAN fibers).

A higher percentage conversion (AI value) means that the stabilized fibers have more ladder polymer. Table I demonstrates that AI values of the stabilized fiber increase with stabilization time (58.7–63.5%), i.e., a longer stabilization time yields a stabilized polymer with greater ladder content. A suitable AI value of stabilized fibers for activating is 50–60%.[14] Figure 4 presents the shift in the X-ray peak of the oxidized fibers with pyrolysis time, suggesting that the structure is altered throughout this period. According to the investigation of AI value (Table I) and structure parameter (Fig. 4), the optimal stabilization was attained at 280°C for 15 min.

Table I presents the elemental content and density of stabilized fibers. The variation in the AI value was very similar to that of the oxygen content. Watt and Johnson[19] evaluated the stabilization of two PAN copolymers, with and without carboxylic acid-containing copolymer, and found that cyclization began from a cyclized ladder polymer. Oxygen combined with the backbone of the ladder polymer eliminated water, yielding a ketone that transformed into hydroxyl pyridine or a pyridine structure. Ko et al. found, based on the AI values, that oxygen absorbed stable ladder polymers with the hydroxyl pyridine or the pyridine structure and demonstrated that lower oxygen content corresponded to less ladder polymer. In this investigation, the carbon and oxygen content is 42.1 and 10.6% in the starting materials, respectively, the oxygen content and the density increase with the time of stabilization and decrease in carbon content (Table I). The carbon content of samples decreases with increases in stabilization time, indicating that the misoriented ladder polymers in stabilized fibers will decrease the formation of carbon basal planes during the stabilization process. It is well known that oxygen is present on the surfaces of stabilized fibers in the form of functional groups and evolves CO and CO_2 gas. Oxygen is introduced as OH and C=O groups and bonded to the carbon backbone of the ladder polymers. Because of the increase in the formation of the ladder polymers during stabilization, the oxygen content of stabilized fibers increased as the thermal treatment time increased. The density of stabilized fibers follows from the structural rearrangements that are associated with cyclization reactions as well as the incorporation of oxygen. The stabilized fiber obtained after 60 min of stabilization has high density, revealing that the stabilization of the fiber increases with ladder polymer content and oxygen content. The fiber diameter declines as the stabilization time increases because of the noncarbon elements that are removed as volatiles and the shrinkage of fibers during the stabilization. The average fiber diameter produced at a stabilization time of 15 min was 4.47 μm. The average fiber diameter that was produced at the stabilization time of 60 min was 4.11 μm.

Properties of ultra-thin PAN-based activated carbon fibers

Analysis of elemental component and density

Following stabilization, fibers were all heated to 1000°C before steam was introduced in the physical activation stage. Table II plots the burn-off and the results of the elemental analysis of ACF as functions of activation time. Upon each treatment of the ACFs, the reaction between carbon and regenerated gas caused the weight loss of the fiber, the weight loss was ~ 49–56 wt % and the corresponding carbon yield at activation times from 0.75 to 15 min was in the range 85–92%. The carbon content of ACFs increased with activation time, but the nitrogen content of ACFs was negatively related to the activation time. This result demonstrates that nitrogen continues to be eliminated from the stabilized fibers during activation, and carbon monoxide is formed by the reaction of carbon constituent of the stabilized fiber with steam, reducing the weight of the emerging ACFs. The formation of new carbon basal planes and the evacuation of a large amount of nitrogen were continuous during activation, increasing the carbon content.

Table II presents the variation in the density of ultra-thin PAN-based ACFs, which is further evidence of the degradation of carbon basal planes by steam during activation. For all fibers, the elimination of nitrogen, the packing of new carbon basal

TABLE II
Preparing Condition, Burn-Off, Elemental Contents, and Density of ACFs

Activation temperature (°C)	Development time (min)	Burn-off (wt %)	Density (g/cm^3)	Elemental contents (%)		
				C	N	O (diff.)
1,000	0.75	49.2	1.94	85.5	10.4	4.1
	5	50.2	2.07	87.7	8.3	4
	10	52.1	2.18	91.4	5.1	3.5
	15	55.2	2.38	91.6	4.4	4

planes, and the degradation of carbon structure are simultaneous. During degradation, the formations of new carbon basal planes were sufficiently fast to outpace degradation and increased the number of carbon basal planes to saturation. During the formation of new carbon basal planes, the open pores become closed, reducing the density of the fibers as the passages through open pores are blocked by new carbon basal planes, since during reaction, the closure of fiber surface inside the structure was impeded. During activation, steam reacted with the new carbon planes on the surface of ACFs. Activation eliminated these blockages, and closed pores in ACFs became open again. The density of ACFs increased with activation time, from 1.94 to 2.38 g/cm^3, revealing that the porosity of fibers increased with the period of activation in steam.

Crystalline structure

Molleyre and Bastick[20] suggested that attack by oxygen causes original pores in fibers to dilate and grow coarse. Increasing the number of defects in a fiber can facilitate attack by oxygen. The variation of *Lc* and d_{002} of ACFs, plotted in Figure 5, demonstrate that as the activation time increases, the graphite-like layer spacing (*d*-spacing) of fibers declines from 0.3581 to 0.3482 nm. However, the crystalline stack height slowly increases from 0.9478 to 2.0772 nm. A fiber activated with steam has a smaller spacing between the graphite-like layers than that in stabilized fibers. Because of the initial removal by oxygen of noncrystalline carbon from the crystal edges of stabilized fibers and the erosion of the crystalline carbon layer, the crystalline stack height gradually increase during the activation immediately thereafter. Accordingly, the crystalline stack height increased as the noncrystalline carbon was removed. Since activation occurs at the high temperature of 1000°C, elemental analysis (Table II) confirmed that following activation by steam, the nitrogen content in the fibers slowly declined, forming and restacking a graphite-like structure to increase the crystalline stack height.

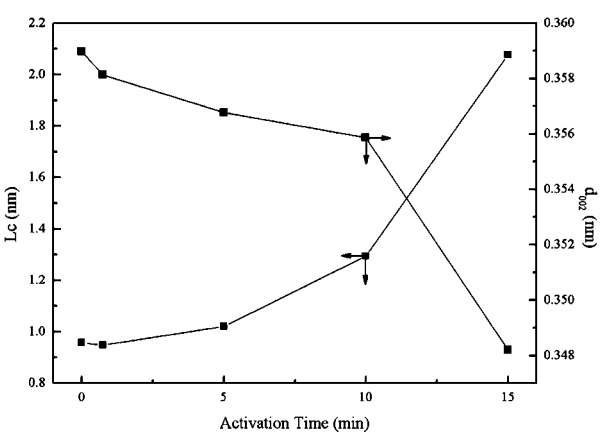

Figure 5 Stacking size (*Lc*) and *d*-spacing (d_{002}) of ACFs as a function of activation time.

Pore structure and surface area of activated carbon fibers

The removal of impurities from gases and liquids by porous carbon proceeds by adsorption, and activation simply increases the internal surface area of carbon, and thereby the number of sites available for adsorption.[20] Both pore size and surface chemistry determine the adsorption properties of ACFs. The adsorption of nitrogen, because of the relatively small molecular diameter of nitrogen, is often exploited at 77 K to determine the porosity and surface area and in a standard procedure for characterizing of porous structures of carbonaceous adsorbents. The adsorption isotherm offers information about the porous structure of absorbent, the heat of adsorption, and its physical and chemical characteristics. The definition of pore size is consistent with the recommendations of IUPAC as follows: micropores have widths of less than 2 nm, mesopores have widths from 2 to 50 nm, and macropores have widths of larger than 50 nm. Micropores can be divided into ultramicropores (width less than 0.7 nm) and supermicropores (width from 0.7 to 2 nm).[21] ACFs are characterized by obtaining adsorption/desorption isotherms produced, and comparing these isotherms against standard isotherms. Type I isotherms exhibit enhanced adsorbent–adsorbate interactions in micropores with molecular dimensions. A narrow range of relative pressures that is required to reach the plateau offers a clue to a limiting pore size. Type II isotherms reveal the formation of adsorbed layer whose thickness continually increases

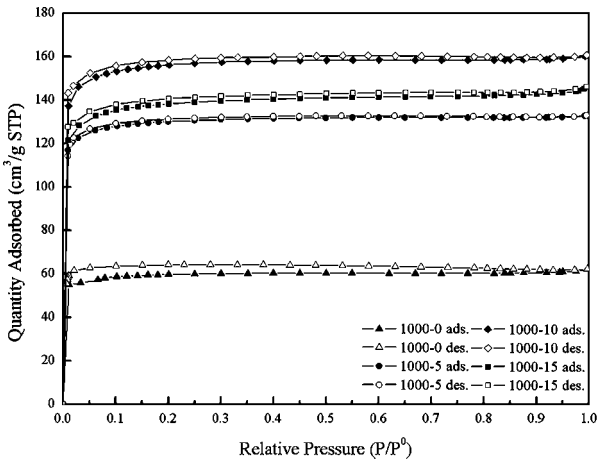

Figure 6 Adsorption–desorption isotherms of ACFs with different activation time. Open symbols, adsorption; full symbols, desorption.

with relative pressure, these are obtained with nonporous or macroporous adsorbents and complete reversal of isotherms possible. Type III isotherms reveal weak adsorbent–adsorbate interactions. Type IV isotherms are closely related to Type II but exhibit a hysteresis loop that is generally related to the filling and emptying of mesopores by capillary condensation. Type V isotherms, like Type III, reveal a weak adsorbent–adsorbate interaction, but the hysteresis loop is associated with pore filling and emptying. Type VI isotherms reveal layer-by-layer adsorption on a highly uniform surface with shape system and temperature-dependent.

Nitrogen adsorption isotherms of ultra-thin PAN-based ACF samples are of Type I in the Brunauer, Deming, Deming, and Teller (BDDT) classification,[16] as presented in Figure 6. Type I isotherms have a nearly horizontal plateau, which may cut the $P/P_0 = 1$ axis sharply and include a ''tail'' near saturation pressure. The initial part of Type I isotherms for carbonaceous adsorbents represents micropore filling. The slope of the plateau at high relative pressure is determined by multilayer adsorption on the nonmicroporous surface, i.e., in mesopores, in macropores, and on the external surface. From this standpoint, one can perceive ACFs as essential microporous adsorbents in this study.

Table III presents the effect of the activation time on the porous structure parameters of ACFs that were prepared at a temperature of 1000°C for 0.75, 5, 10, and 15 min. Specific surface area of the ACFs was calculated using the BET method (P/P_0 between 0.05 and 0.20). The surface areas of the stabilized fibers increased remarkably after the activation process. During the activation process, steam etched the carbon basal planes of stabilized fibers, and this reaction promoted degradation of the structures and formed new flaws. Therefore, the surface area of fiber increased remarkably after activation. The specific surface area of ultra-thin ACFs increased with activation time to the maximum at 10 min (1408 m^2/g), and thereafter declined. The loss of volatile components and the subsequent reorganization of the remaining structures are widely known to increase surface areas and porosity. The experimental results suggest that activation continues with activation time, increasing the number and size of the pores in ultra-thin ACFs. An activation time of 10 min was optimized for porosity; a longer period results in the incorporation of small pores, such that larger pores are formed (whose diameter exceeds that of the small pores), reducing the surface area.

Table III demonstrates that the total pore volume increases from 0.249 to 0.797 cm^3/g with activation time from 0.75 to 15 min. Increasing the activation time widened the micropores, destroying the walls between the adjacent pores, enlarging them reducing the fractional micropore volume, and increasing the total pore volume. Samples are activated at 1000°C; the micropore volume of ACFs obtained from 15 min is less than that after an activation time of 10 min (0.624 vs. 0.687 cm^3/g). The ratio of micropore volume to total pore volume in ACFs increases with activation time and peaks at 87.9% after 10 min, and that of the samples generated at an activation time

TABLE III
Porous Structural Parameters of PAN-Based ACFs

Activation time (min)	S_{BET} (m^2/g)	D_{aver} (nm)	Pore volume		
			V_{tot} (cm^3/g)	V_{mi} (cm^3/g)	V_{mi}/V_{tot} (%)
0[a]	10	1.4	0.006	0.002	33.3
0.75	668	1.49	0.249	0.212	85.1
5	854	1.63	0.347	0.300	86.5
10	1408	2.22	0.782	0.687	87.9
15	1081	2.95	0.797	0.624	78.3

Note: S_{BET}, specific surface area; V_{tot}, total pore volume; V_{mi}, volume of micropore; D_{aver}, average pore diameter.
[a] Properties of fibers obtained from stabilized fibers.

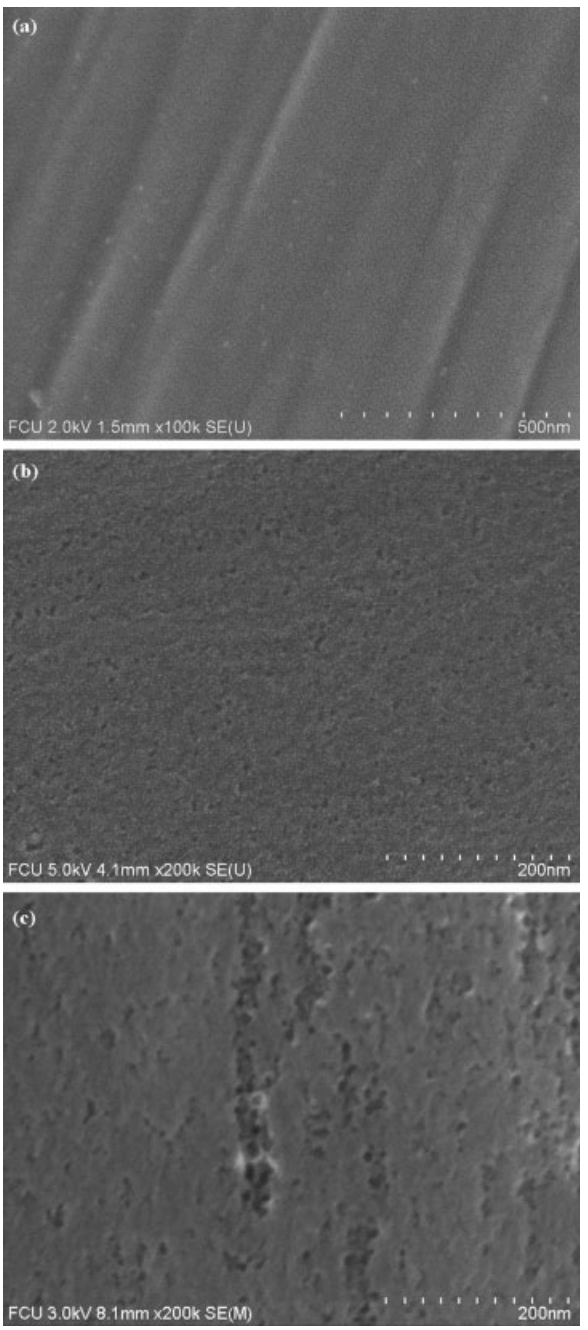

Figure 7 FESEM photographs of fibers prepared at (a) after oxidization, (b) 10 min activation, and (c) 15 min activation.

of 15 min is lower. The samples prepared with 15 min of activation have a higher total pore volume and a lower ratio of micropore volume to total pore volume, suggesting that a longer activation time generates more new pores and widens micropores to form mesopores. Table III presents the mean pore diameter, which increases from 1.49 to 2.95 nm over the range of activation times. The loss of volatile components and the subsequent reorganization of the residual structure are responsible for the porosity; long activation produced mesopores and reduced the surface areas of the resultant ACFs.

Morphology of activated carbon fibers

Figure 7 presents the FESEM of surface structures that were prepared from oxidized and activated fibers. The micrographs from Figure 7(a) reveal that stabilized fibers have quite a smooth surface without any pores except for some occasional cracks, suggesting that oxidized fibers have passed through a plastic phase during the heating treatment that was conducted to restructure the surface. Figure 7(b,c) present ACFs formed with various activation times at higher magnifications, which demonstrate that the surface morphology is cracked and porous. Activation at 1000°C for 10 min generated ACFs with a high degree of porosity and the maximum surface area (1408 m^2/g). Small cracks and micropores, which are visible in Figure 7(b), and mesopores formed from micropores, as presented in Figure 7(c), during the gasification phase cause loss of carbon. This loss of carbon causes pore widening and the development of mesoporosity.

CONCLUSIONS

In this investigation, ultra-thin PAN fibers were stabilized and activated, and the effect of stabilization time on the physical properties and elemental composition of fibers was evaluated. Stabilization was optimal at 280°C for 15 min in an atmosphere of air. Fibers were then activated with steam at 1000°C by varying the activation time. The experimental results are as follows: (1) the burn-off, the carbon content, the density, and the *Lc* value of ACFs increased with activation time, and d_{002} and the diameter declined; (2) adsorption isotherms for ultra-thin PAN-based ACFs are of Type I isotherms according to the BDDT classification, as in micropore filling; (3) the maximum BET surface area and micropore volume were 1408 m^2/g and 0.687 cm^3/g, respectively, upon activation at 1000°C for 10 min; (4) increasing the activation time creates more new pores and widens some of the micropores to form mesopores, increasing the total pore volume and reducing the ratio of the micropore volume to total pore volume.

References

1. Dubinin, M. M.; Polyakov, N. S.; Petukhova, G. A. Adsorption Sci Technol 1993, 10, 17.
2. Alcaniz-Monge, J.; Cazorla-Amoris, D.; Linares-Solano, A.; Yoshida, S.; Oya, A. Carbon 1994, 32, 1277.
3. Chosal, R.; Kaul, D. J.; Boes, U.; Sanders, D.; Smith, D. M.; Maskara, A. Mater Res Soc Symp Proc 1995, 371, 413.
4. Sakoda, A.; Suzuki, M.; Hirari, R.; Kawano, K. Water Res 1991, 25, 219.

5. Mochida, I.; Korai, Y.; Shirahama, M.; Kawano, S.; Hada, T.; Seo, Y.; Yoshikawa, M.; Yasutake, A. Carbon 2003, 38, 227.
6. Miyake, Y.; Suzuki, M. Gas Sep Purif 1993, 7, 229.
7. Yoshida, A.; Tanahashi, I.; Nishino, A. Carbon 1990, 28, 611.
8. Shimazaki, K.; Hirai, M. Nippon Kagaku Kaishi 1992, 7, 739.
9. Otani, S.; Kokubo, Y.; Koitabashi, T. Bull Chem Soc Jpn 1970, 43, 3291.
10. Tang, M. M.; Bacon, R. Carbon 1964, 2, 211.
11. Arons, G. N.; Macnair, R. N. Text Res J 1972, 42, 60.
12. Freeman, J. J.; Tomlinson, J. B.; Sing, K. S. W.; Theocharis, C. R. Carbon 1995, 33, 795.
13. Ishizaki, N. Chem Eng 1984, 29, 496.
14. Ko, T. H.; Ting, H. Y.; Lin, C. H. Appl Polym Sci 1988, 35, 631.
15. Brunauer, S.; Emmett, P. H.; Teller, E. J Am Chem Soc 1938, 60, 309.
16. Gregg, S. J; Sing, K. S. W. Adsorption, Surface Area and Porosity; Academic Press: New York, 1982.
17. Fitzer, E.; Müller, D. J. Carbon 1975, 13, 63.
18. Uchida, T.; Shinoyama, I.; Ito, Y.; Nukuda, K. Carbon 1971, 15, 31.
19. Watt, W.; Johnson, W. Nature 1975, 257, 210.
20. Molleyre, F.; Bastick, M. Carbon 1976, 76, 500.
21. Wigmans, T. Carbon 1989, 27, 13.